

Article

First-Principles Investigations of the Electronic Structure and Mechanical Characteristics of Nd³⁺-Doped YAlO₃ Crystals

Shuai Meng ¹, Aocheng Li ¹, Kun Li ^{1,*}, Yanjie Song ², Zhenxing Qin ¹, Rui Zhang ¹, Yufei Zhang ¹, Weijie Ren ¹ and Wen Yang ³

¹ School of Applied Science, Taiyuan University of Science and Technology, Taiyuan 030024, China

² Key Laboratory of Solid State Laser, Technical Institute of Physics and Chemistry, Chinese Academy of Sciences, Beijing 100190, China

³ School of Materials Science and Engineering, Taiyuan University of Science and Technology, Taiyuan 030024, China

* Correspondence: likun@tyust.edu.cn

Abstract: Near-infrared laser radiation based on Nd³⁺-doped yttrium ortho-aluminate (Nd:YAlO₃, Nd:YAP) has garnered significant interest regarding solid-state lasers. Nevertheless, the crystal microstructures and electronic characteristics of Nd:YAP are still unclear, and the unique physical properties underlying its enormous applications require clarification. In this study, we conducted first-principles calculations at the atomic level to explore the electronic properties and mechanical characteristics of both pure YAP and Nd³⁺-doped YAP. The results suggest that the substitution of the Y³⁺ ion site with the Nd³⁺ impurity ion induces slight structural distortion in the YAP crystal lattice. An impurity band emerges between the original conduction band and the valence band, attributed to the 4f orbital of the Nd³⁺ ion, exerting a substantial influence on the narrowing of the band gap. Through an analysis of the mechanical characteristics of both pure YAP and Nd:YAP, we conclude that the incorporation of Nd³⁺ atoms leads to a reduction in the mechanical properties of YAP to a certain extent. Our study can serve as a foundational data source for investigations into material performance, especially for the application of Nd:YAP in solid-state laser systems.

Keywords: near-infrared laser; first-principles calculations; electronic structure; Nd:YAlO₃



Citation: Meng, S.; Li, A.; Li, K.; Song, Y.; Qin, Z.; Zhang, R.; Zhang, Y.; Ren, W.; Yang, W. First-Principles Investigations of the Electronic Structure and Mechanical Characteristics of Nd³⁺-Doped YAlO₃ Crystals. *Crystals* **2024**, *14*, 293. <https://doi.org/10.3390/cryst14040293>

Academic Editor: Sawanta S. Mali

Received: 28 February 2024

Revised: 14 March 2024

Accepted: 19 March 2024

Published: 22 March 2024



Copyright: © 2024 by the authors. Licensee MDPI, Basel, Switzerland. This article is an open access article distributed under the terms and conditions of the Creative Commons Attribution (CC BY) license (<https://creativecommons.org/licenses/by/4.0/>).

1. Introduction

In the field of solid-state lasers, luminescence at a wavelength of approximately 1 μm is imperative for various applications spanning industry, medicine, military, and non-linear frequency generation [1–5]. Yttrium ortho-aluminate (YAlO₃, YAP) with a perovskite-type structure serves as an excellent host for various rare-earth (RE) ions. These materials find extensive use owing to their favorable characteristics, including high thermal conductivity, exceptional thermo-mechanical properties, low cost, large-size fabrication, and ease of manufacturing [6]. Among the various rare-earth (RE) ions, neodymium (Nd) ions have garnered significant attention due to their inherent advantages, including high quantum efficiency, broad absorption bands, and long radiative lifetimes [7]. Upon doping with rare-earth Nd³⁺, YAP emerges as an important candidate for generating 1 μm laser radiation. Numerous studies have suggested that Nd:YAP is a promising alternative crystal to Nd:YAG for achieving high power output. Observations reveal that the Nd:YAP crystal exhibits a large stimulated emission cross-section, excellent optomechanical coefficient, and high thermal conductivity [8,9]. Notably, the intrinsic birefringence and distinctive optical anisotropy of the Nd:YAP host effectively mitigate thermal depolarization, enabling the generation of a linearly polarized laser without the need for additional polarizing devices in the laser cavity [10]. Hence, the development of laser sources utilizing the Nd:YAP crystal holds significant practical value.

The evolution of the Nd:YAP laser has a rich history, and scientists have contributed to its development through rigorous experimentation, theoretical advancements, and technological innovations. For the first time, Wu et al. demonstrated a compact Q-switched operation of a diode-pumped Nd:YAP laser with a 90 W output. They attained a 4.1 W output at 3.5 μm from an optical parametric oscillator pumped within the cavity of a Q-switched, diode-pumped Nd:YAP laser operating at a frequency of 10 kHz [11]. Wei et al. analyzed the energy level transitions and polarization properties of Nd:YAP crystals, and an a-axis, polarized, 1339 nm pulse laser was successfully constructed with pulse width and full width at half maximum of 180 μs and 35 ns, respectively. Their efforts in polarization selection to achieve oscillation in weak lines are noteworthy for anisotropic Nd:YAP laser crystals, allowing for the specific targeting of particular transitions [12]. By the floating zone method, Yanagida et al. synthesized and evaluated Nd-doped YAP crystals. After crystal growth, the optical properties, including transmittance, photoluminescence spectra, and photoluminescence decay curves, and scintillation properties, such as pulse height spectra, light yield nonproportionalities, and energy resolutions, were systematically investigated, indicating the potential application of Nd:YAP in scintillation detectors [13]. Recent investigations have tended to focus on exploring the cryogenic laser applications of Nd:YAP [8,14]. By studying the structural, thermal, and spectroscopic properties of Nd:YAP under cryogenic temperatures, an interesting zero-thermal-expansion phenomenon has been observed around 180 K, which could significantly suppress wavefront distortion in high-power lasers [8]. Furthermore, authors have investigated the laser performance of an a-cut rod of Nd:YAP crystal as the gain medium for zero thermal expansion around 180 K. The study encompassed laser performance across a temperature range from 80 to 290 K. At the critical temperature of zero thermal expansion (180 K), the authors achieved maximum output power with minimal threshold pump power and the highest optical-to-optical conversion efficiency. Additionally, a reduction in both thermal lensing and wavefront distortion effects was achieved without the need for an additional optical correction system. These findings present innovative solutions for generating high-power and high-beam-quality lasers using zero thermal expansion gain materials, such as Nd:YAP crystals. The aforementioned investigations underscore the significance of research on Nd:YAP crystals [14]. Although there are a lot of experimental studies on Nd³⁺-doped YAP crystals, the new characteristics and the specific influence of impurity ions on the system remain unclear. To the best of our knowledge, there are few systematic studies on the microstructural, electronic, and mechanical properties of Nd³⁺-doped YAP at the atomic level.

In this study, we investigated the microstructure of both pure and Nd³⁺-doped YAP by performing first-principles calculations. Additionally, based on the obtained structure, we calculated and analyzed the band structure and density of states to gain deeper insights into the electronic properties. In order to provide a better description of the electronic structure of Nd-doped YAP, we conducted further calculations using the LDA+U method (including spin-orbit effects) for comparison. Furthermore, we also calculated the mechanical properties of the Nd³⁺-doped YAP system. The elastic constants C_{ij} , elastic moduli (B, G, E), Pugh's ratio, Poisson's ratio, hardness, and elastic anisotropy were investigated. The present results provide an essential understanding of rare-earth ion-doped lasing materials. Our study can serve as a foundational data source for investigations into material performance, especially for the application of Nd:YAP in solid-state laser systems. The structure of this paper is outlined as follows: Section 2 delineates the computational materials and methods employed. In Section 3, an analysis of the derived structural, electronic, and mechanical properties is presented. Lastly, a summary and conclusion are provided.

2. Materials and Methods

YAP possesses a distorted perovskite structure belonging to the orthorhombic $Pbnm$ space group, with lattice parameters of $a = 5.180 \text{ \AA}$, $b = 5.330 \text{ \AA}$, $c = 7.375 \text{ \AA}$, and $\alpha = \beta = \gamma = 90^\circ$ [15]. The conventional unit cell of YAP contains four AlO_6 octahedra formula units. The Al ions are located in the center of the AlO_6 and Y ions occupy the holes between them.

To investigate the influence of Nd ions on the microstructure and material properties of YAP crystals, we constructed a $2 \times 2 \times 1$ supercell with up to 80 atoms, of which one Y^{3+} ion was replaced by Nd^{3+} . The concentration of Nd^{3+} was equal to 6.25%, which was close to the experimental data reported by Basavalingu et al. [16]. In the crystal lattice, the Nd^{3+} ion possessed similar electronic configurations and radius to Y^{3+} and could naturally incorporate into the YAP host matrix and easily substitute the position of Y^{3+} [17]. The structure of Nd:YAP is illustrated in Figure 1. The Nd^{3+} impurity was surrounded by eight O^{2-} and constituted a $[\text{NdO}_8]^{13-}$ local structure.

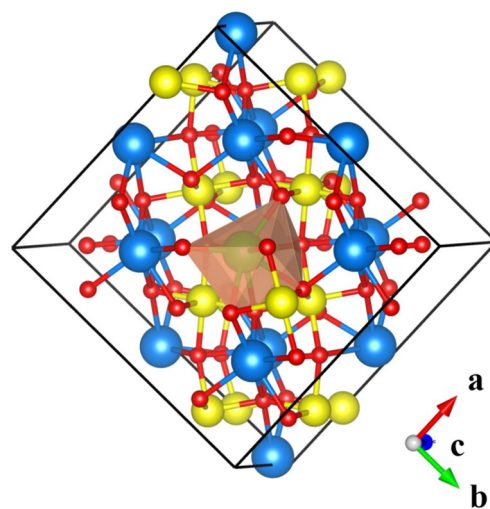


Figure 1. The structure of $2 \times 2 \times 1$ supercell of YAP with Nd^{3+} ion substituted for Y^{3+} ion. Nd dopant is shown as a green ball and the blue, yellow, and red spheres represent Y, Al, and O atoms, respectively.

Our calculations were performed with the Cambridge Serial Total Energy Package (CASTEP) code, which is based on the plane-wave pseudo-potential density functional theory method [18]. A large number of successful simulations, spanning surface chemistry, bond structure, density of states, and optical properties, have been accomplished through the utilization of the CASTEP code. This computational tool finds applicability in the domains of solid physics, materials science, chemistry, and chemical engineering and offers the potential for cost savings and expedited development cycles compared to experimental approaches. The exchange–correlation effects were treated within the generalized gradient approximation (GGA) with the Perdew–Burke–Ernzerhof (PBE) function [19]. $\text{Y-}4d^15s^2$, $\text{Al-}3s^23p^1$, $\text{O-}2s^22p^4$, and $\text{Nd-}4f^45s^25p^66s^2$ were treated as atomic valence electrons; the other states were kept frozen as core and semi-core states. Through the convergence tests, a cut-off energy of 500 eV with fine Monkhorst–Pack k meshes was adopted. The convergences of the energy, maximum force tolerance, maximum atomic displacement, and maximum stress component were $2 \times 10^{-5} \text{ eV/atom}$, 0.05 eV/\AA , 0.002 \AA , and 0.1 GPa , respectively. To ensure that our modeling could reproduce the basic crystal parameters of ideal, pure YAP and Nd-doped YAP, the computer simulation started with complete geometry optimization.

3. Results and Discussion

3.1. Structure

Before property calculations, geometry optimization was necessary to obtain fully stable structures of both YAP and Nd:YAP. The obtained lattice parameters of pure YAP and Nd:YAP are summarized in Table 1, together with the experimental and theoretical results.

With the incorporation of the Nd³⁺ impurity ion, Nd:YAP exhibited slight structural distortions, and the lattice volume experienced a certain degree of expansion. This phenomenon could be ascribed to the larger atomic radius of Nd³⁺ (0.98 Å) compared to that of Y³⁺ (0.90 Å) [20]. The calculated lattice parameters were overvalued compared to the experimental lattice parameter, which was attributed to the use of the PBE functional. However, it is noteworthy that the deviation between the experimental and our theoretical values was below 2%, justifying the rationality of our calculation scheme and chosen parameters.

Table 1. The lattice constants (a, b, c) and cell volume (V) of the optimized YAP and Nd:YAP compared with experimental data.

Structure	Source	a (Å)	b (Å)	c (Å)	V (Å ³)
YAP	This work	5.216	5.400	7.440	209.538
	Exp. [21]	5.180	5.330	7.375	203.619
	Cal. [22]	5.210	5.359	7.427	207.365
	Cal. [15]	5.310	5.413	7.537	216.636
Nd:YAP	This work	5.229	5.401	7.449	210.334
	Exp. [16]	5.162	5.353	7.391	204.229

To further clarify the structure of the Nd³⁺-doped YAP crystal, we also simulated the X-ray diffraction (XRD) patterns of pure YAP and Nd:YAP theoretically. X-ray diffraction (XRD) analysis is a methodology that leverages the diffraction phenomenon of X-rays in crystalline materials for the purpose of elucidating material structures. Widely employed, this technique plays a pivotal role in exploring intricate crystal structures across diverse systems. The calculated results are shown in Figure 2, together with the available experimental result of pure YAP [16]. The simulated XRD spectra of Nd:YAP are shown as a red line and the black and blue lines represent pure YAP and the available experimental result of pure YAP (JCPDF#70-1677), respectively. Taking into account the distribution of relative intensities, the simulated spectra in the 2θ range from 20 to 70° exhibited overall good agreement with the available experimental data, thus affirming the accuracy of our simulation. Our simulated XRD spectra for Nd:YAP can serve as valuable guidelines for future experimental syntheses.

3.2. Electronic Properties

Electronic band structure and density of states (DOS) often provide sufficient information for a comprehensive characterization of a material's electronic properties. The calculated band structures for pure YAP and Nd:YAP are depicted in Figure 3. Our primary focus was on the distribution of energy bands near the Fermi energy level. The most notable distinction, in comparison to pure YAP, lay in the presence of occupied states near the Fermi level. It was concluded that the incorporation of the Nd³⁺ ion into the YAP host crystal led to a narrowing of the band gap. Notably, Ju M. et al. observed analogous outcomes in the Nd:Y₂O₃ and Cr:YAP systems [23,24]. The calculated indirect band gap of YAP was 5.7 eV, demonstrating reasonable agreement with earlier first-principles calculations [25]; yet, it remained lower than the experimental value of 7.1 eV [26]. Such a discrepancy between theory and experiment is expected when the density functional theory method is used.

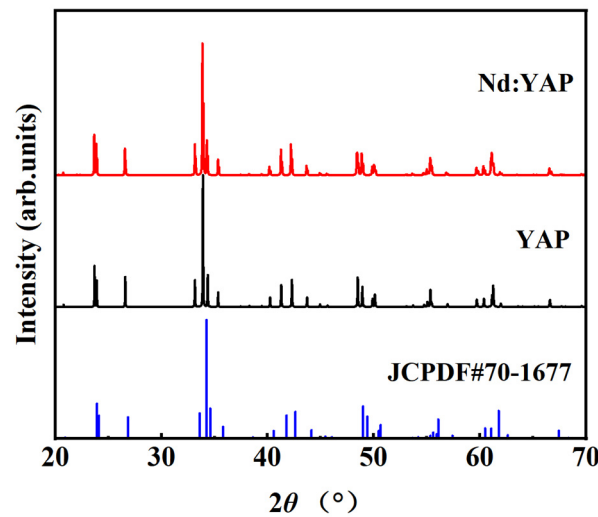


Figure 2. Simulated XRD patterns of YAP and Nd:YAP, along with the experimental pattern of pure YAP. The simulated XRD spectra of Nd:YAP are shown as a red line and the black and blue lines represent pure YAP and the available experimental result of pure YAP (JCPDF#70-1677), respectively.

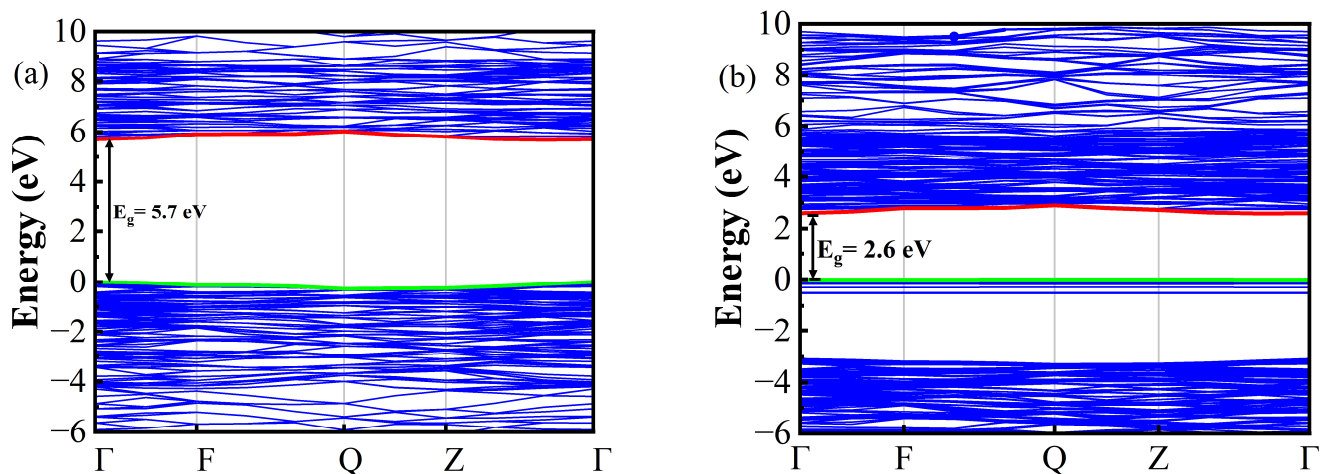


Figure 3. The calculated band structures of (a) pure YAP and (b) Nd:YAP. The red line represents the conduction band minimum, and the green line represents the valence band maximum.

For a comprehensive understanding of the electronic properties, we additionally calculate the partial DOS for YAP and Nd:YAP. The influence of each atom on the entire density of states could be seen from the partial DOS. Figure 4 shows the calculated partial density of states of YAP and Nd:YAP, offering a visual representation of the partial DOS for the two materials. In YAP, O and Y atoms played a decisive role in the band structure near the Fermi level, and the band gap width was mainly determined by the O-2p and Y-4d states. The valence band of YAP came from the O-2p state, with a small amount of Y-4d state mixed with Al-3s and Al-3p states. The conduction band above the Fermi level was mainly dominated by the Y-4d state, which had a significant impact on the properties of YAP. Compared to pure YAP, the density of states of Nd:YAP could be divided into three parts near the Fermi energy level, which were mainly contributed to by the O-2p, Nd-4f, and Y-4d states. The O-2p states played a major role below the Fermi level, whereas the conduction band was mainly formed by the Y-4d states, and the Al atom had a weak contribution near the Fermi energy level. It is noteworthy that a new peak emerged above the Fermi energy level, originating from the Nd-4f states. Therefore, the band gap narrowing feature could be ascribed to the Nd³⁺ dopant ion in YAP. This narrowing of the band gap was indicative of changes in the electronic structure that may have led to

enhanced optical or electrical properties in Nd:YAP, making it a potentially useful material for various applications. Overall, the detailed analysis of the partial DOS provided valuable insights into the electronic properties of YAP and Nd:YAP, laying the foundation for further explorations of their potential applications.

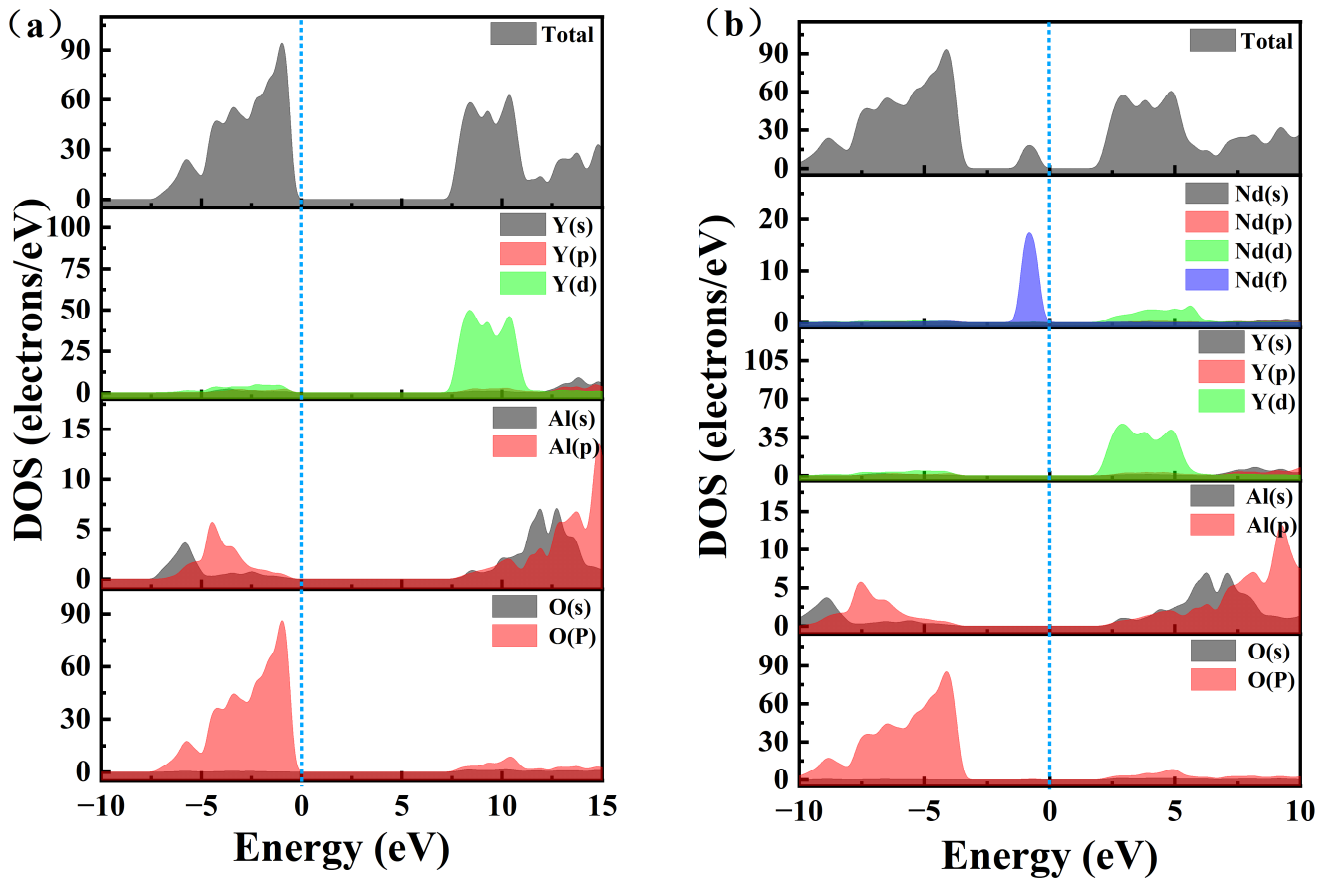


Figure 4. The calculated total and partial DOS of (a) YAP and (b) Nd:YAP; the Fermi level is indicated by the dashed line.

Electronic transitions significantly impact the optical properties of materials. Moreover, the absorption spectrum and refractive index of Nd:YAP play a crucial role in laser applications. Based on the calculated electronic band structure, we also conducted a preliminary study of the optical properties of YAP materials before and after doping. The calculated results are presented in Figure 5, where a scissor operator of 1.4 eV was used to eliminate the difference between the theoretical and experimental gap values. The main function of the scissor operator was to adjust the theoretically calculated bandgap value to be consistent with the experimental value, without changing the detailed characteristics of the energy band.

Figure 5a clearly shows that in Nd:YAP, a distinct optical absorption band emerged at approximately 2.5 eV. Notably, a small absorption peak also appeared at 1.5 eV, which was in excellent agreement with the pump source wavelength of 803 nm in Nd:YAP. The absorption band of the YAP materials from ultraviolet to infrared expanded with the incorporation of Nd³⁺ ions. This phenomenon was attributed to the doping of rare-earth ions in the host crystals. Figure 5b illustrates that the refractive index of Nd:YAP exhibited an increase in comparison to pure YAP. The calculated refractive index of Nd:YAP was 1.955 (@1064 nm), demonstrating close agreement with the experimental value of 1.929 (@1064 nm) [2] and affirming the high accuracy of our calculations. This led to the conclusion that the alterations in the optical properties were intricately linked to the 4f

states of the Nd^{3+} ions. Our current findings offer valuable insights into the trends of optical properties within the Nd:YAP system.

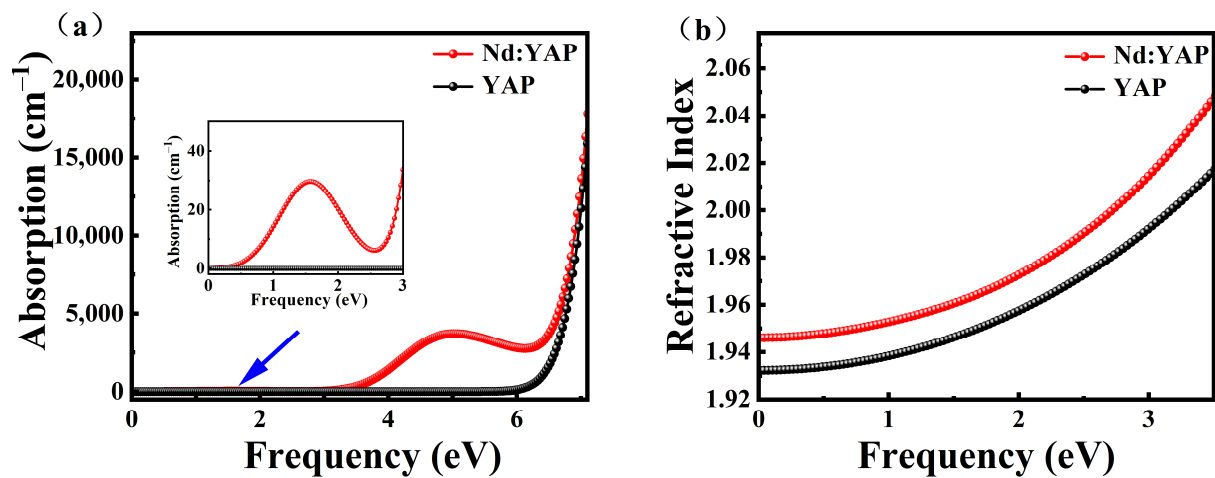


Figure 5. The optical properties of YAP and Nd:YAP. The (a) absorption coefficient spectrum and (b) refractive index in the (1 0 0) direction.

However, the standard density functional theory calculations using the GGA method may not have accurately described the strongly correlated 4f electrons of Nd atoms. In order to provide a better description of the electronic structure of Nd-doped YAP, the band structures and the total DOS of Nd:YAP were further calculated using the LDA+U method (including spin–orbit effects). The U value of Nd has been determined to be 6 eV by Herbst [27].

Figure 6 shows the calculated electronic band structures and total DOS of Nd:YAP obtained by the LDA+U method, including spin–orbit effects, and the Fermi level is indicated by the dotted line. The results suggest a gap value of 4.1 eV for Nd^{3+} -doped YAP, exerting a substantial influence on the narrowing of the band gap. Similar behaviors also have been observed in the aforementioned Nd:Y₂O₃ and Cr:YAP systems [23,24].

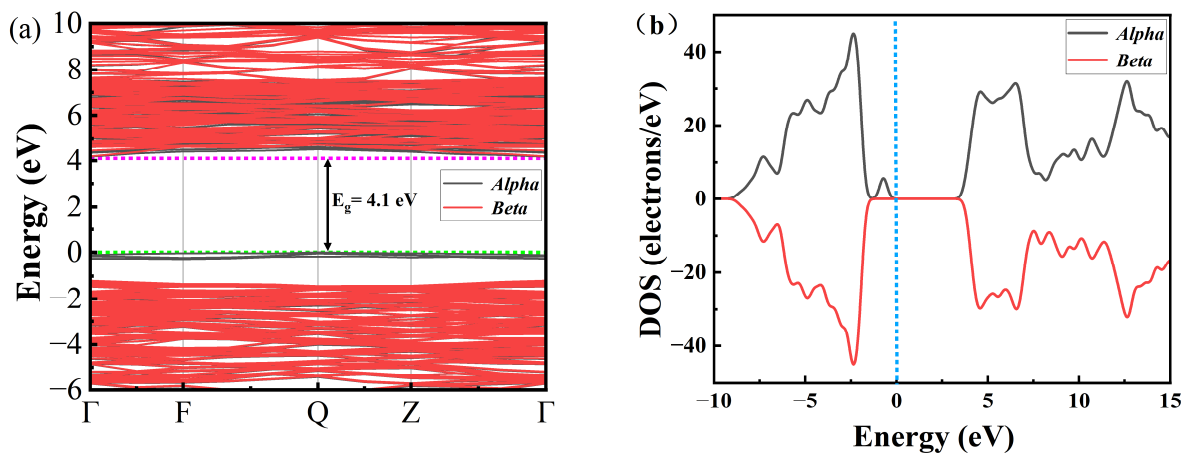


Figure 6. The (a) calculated band structure and (b) total DOS of Nd:YAP using LDA+U method (including spin–orbit effects). The Fermi level is indicated by the dotted line.

Through a comparative analysis employing the GGA+PBE and LDA+U methods, an investigation into the electronic properties, including band structure and density of states, was conducted. However, there was not any available information on band gap values for Nd:YAP in the literature to be compared with our obtained results. Thus,

we hope that our theoretical results will provide more available information for further experimental investigations.

3.3. Mechanical Properties

The investigation of the mechanical properties of materials, including elastic constants, modulus, Poisson's ratio, and hardness, holds immense importance for the industrial utilization of materials, particularly in the realm of lasers. For this purpose, we conducted a comprehensive investigation into the mechanical properties of Nd³⁺ ion-doped YAP.

As we know, the elastic constant (C_{ij}) determines the stiffness of a crystal against an externally applied strain. In our study, based on the general Hooke's law, the elastic constant was obtained by employing the strain–stress method. The ortho crysorbombital possesses nine independent elastic constants, denoted as C_{11} , C_{22} , C_{33} , C_{12} , C_{13} , C_{23} , C_{44} , C_{55} , and C_{66} . Additional constants can be determined by symmetry relationships: $C_{12} = C_{21}$, $C_{13} = C_{31}$, and $C_{23} = C_{32}$; the rest are set to zero [28]. Before considering the elastic properties, the Born mechanical stability of these systems should be examined. Mechanical stability criteria for the orthorhombic phase are given by the below [28]:

$$\begin{aligned} C_{11} > 0, C_{11}C_{22} > C_{12}^2, \\ C_{11}C_{22}C_{33} + 2C_{12}C_{13}C_{23} - C_{11}C_{23}^2 - C_{22}C_{13}^2 - C_{33}C_{12}^2 > 0, \\ C_{44} > 0, C_{55} > 0, C_{66} > 0. \end{aligned} \quad (1)$$

The computed elastic constants C_{ij} for YAP and Nd:YAP at zero temperature and zero pressure are presented in Table 2, alongside additional YAP calculations [15]. The obtained elastic constants satisfied the mechanical stability criteria and indicated that our computational models were mechanically stable.

Table 2. Calculated elastic constants C_{ij} of YAP and Nd:YAP.

Structure	Source	C_{11}	C_{22}	C_{33}	C_{12}	C_{13}	C_{23}	C_{44}	C_{55}	C_{66}
YAP	This work	322.6	273.1	322.9	110.7	120.0	115.8	148.7	135.4	94.1
	Cal. [15]	337.0	192.7	285.5	90.4	136.0	99.3	147.7	140.3	80.8
Nd:YAP	This work	324.1	273.8	294.8	96.7	108.1	104.4	141.9	123.3	84.7

Compared with single-crystal elastic constants, polycrystalline elastic properties such as bulk modulus, shear modulus, Young's modulus, and Poisson's ratio usually have higher practical value in the field of lasers. Further, the Voigt–Reuss–Hill approximation can be employed [29], which is often used to calculate the elastic moduli of polycrystals. Relying on the calculated elastic constants, we determined the bulk modulus B , shear modulus G , and Young's modulus E . In addition to the aforementioned moduli, Pugh's ratio and Poisson's ratio can serve as evaluation indices to characterize the mechanical properties of materials. Pugh's ratio, defined as the ratio of bulk modulus B to shear modulus G (B/G), reflects the ductile or brittle behavior of solid materials and is closely tied to the material's subsequent processing performance. In general, a B/G ratio exceeding 1.75 indicates ductility, whereas a lower ratio suggests brittle behavior. Similarly, a Poisson's ratio exceeding 0.26 signifies ductility, while a lower value suggests brittleness.

From Table 3, it can be observed that the computed bulk modulus value for YAP was 178.4 GPa, in close agreement with the practical measurements of 188 GPa and 192 GPa [15], suggesting that both YAP and Nd:YAP exhibited brittle characteristics. Furthermore, the bulk modulus (B), shear modulus (G), Young's modulus (E), Pugh's ratio, Poisson's ratio, and hardness of Nd:YAP slightly decreased compared to pure YAP. Consequently, it was inferred that the introduction of Nd atoms into YAP diminished the mechanical properties of the material to some extent. In the absence of existing reports on the mechanical properties of Nd:YAP, the findings presented herein can serve as valuable references for

subsequent calculations and experiments, particularly within the realms of laser crystal manufacturing and laser system design.

Table 3. Calculated bulk modulus B, shear modulus G, Young’s modulus E (expressed in Gpa), Pugh’s ratio, Poisson’s ratio, and hardness for YAP and Nd:YAP.

Structure	Source	B	G	E	Pugh’s Ratio	Poisson’s Ratio	Hardness
YAP	This work	178.4	111.4	276.5	1.60	0.242	15.14
	Cal. [15]	156.7	100.9	249.2	1.55	0.235	-
	Exp. [30]	188	-	-	-	-	-
	Exp. [31]	192	-	-	-	-	-
Nd:YAP	This work	167.5	106.8	264.3	1.57	0.237	15.07

Figure 7 depicts the calculated directional dependence of Young’s modulus on the XY, XZ, and YZ planes in YAP and Nd:YAP crystals [32], indicating subtle anisotropy in both systems. For isotropic systems, the surface should be spherical, and the deviation from the sphere represents the degree of elastic anisotropy. The universal elastic anisotropy index [33] decreased from 0.23 for YAP to 0.20 for Nd:YAP, indicating an enhancement in elastic isotropy upon the incorporation of Nd atoms into YAP. Given the absence of reports on the elastic constants and polycrystalline elastic properties of Nd:YAP, our results can serve as a reference for future investigations.

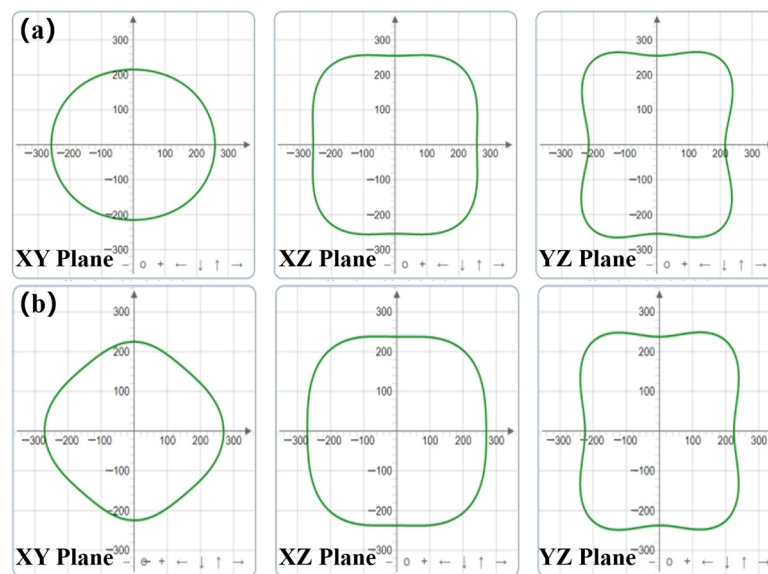


Figure 7. The directional dependent Young’s modulus in different planes for (a) YAP and (b) Nd:YAP. The units are expressed in GPa.

4. Conclusions

In summary, we present a theoretical investigation of the microstructural, electronic, and mechanical characteristics of Nd³⁺-doped YAP crystals using first-principles calculations. Through a comparative analysis employing the GGA+PBE and LDA+U methods, an investigation into the electronic properties, including band structure and density of states, was conducted. The computed results reveal the presence of an impurity band near the Fermi level, attributed to the 4f orbital of the Nd³⁺ ion. This provides clear evidence that the presence of Nd³⁺ impurity ions induces a narrowing of the band gap. The calculated absorption coefficient spectrum and refractive index of Nd:YAP exhibited close concordance with the experimental values, thereby affirming the high precision and accuracy of our calculations. This leads to the conclusion that the alterations in optical properties are

intricately linked to the 4f states of Nd³⁺ ions. Furthermore, through an analysis of the mechanical properties of pure YAP and Nd:YAP, the elastic constants C_{ij} , elastic moduli (B, G, E), Pugh's ratio, Poisson's ratio, hardness, and elastic anisotropy were investigated. It was observed that the incorporation of Nd³⁺ atoms moderately diminished the mechanical characteristics of YAP. The universal elastic anisotropy index decreased for Nd:YAP, indicating an enhancement in elastic isotropy upon the incorporation of Nd atoms into YAP. These investigations underscore the significance of comprehending the relationship between structural, electronic, and mechanical behavior in the field of materials design and engineering. We hope that our findings will furnish valuable insights for the design of future Nd:YAP lasers, particularly within the realms of laser crystal manufacturing and laser system design.

Author Contributions: Conceptualization, S.M. and K.L.; methodology, W.Y.; software, S.M.; validation, A.L., K.L., and S.M.; formal analysis, A.L. and Z.Q.; investigation, R.Z.; resources, Y.S.; data curation, S.M.; writing—original draft preparation, S.M.; writing—review and editing, S.M.; visualization, Y.Z.; supervision, W.R.; project administration, K.L.; funding acquisition, S.M. All authors have read and agreed to the published version of the manuscript.

Funding: This work was supported by the National Natural Science Foundation of China (grant no. 62205349), Science and Technology Innovation Teams of Shanxi Province (no. 202204051001002), Fundamental Research Program of Shanxi Province (grant nos. 202103021224268, 202203021221146, 202203021222207, and 202303021222175), Science and technology innovation plan of colleges and universities in Shanxi Province (grant no. 2022L320), and Taiyuan University of Science and Technology Scientific Research Initial Funding (grant nos. 20222006 and 20222067).

Data Availability Statement: The original contributions presented in this study are included in the article; further inquiries can be directed to the corresponding authors.

Conflicts of Interest: The authors declare no conflicts of interest.

References

1. Rocca, J.P.; Fornaini, C.; Brulat, N.; Samy, B.S.; Darqueceretti, E. CO₂ and Nd:YAP laser interaction with lithium disilicate and Zirconia dental ceramics: A preliminary study. *Opt. Laser Technol.* **2014**, *57*, 216–223. [[CrossRef](#)]
2. Moncorgé, R.; Chambon, B.; Rivoire, J.Y.; Garnier, N.; Descroix, E.; Laporte, P.; Guillet, H.; Roy, S.; Mareschal, J.; Pelenc, D.; et al. Nd doped crystals for medical laser applications. *Opt. Mater.* **1997**, *8*, 109–119. [[CrossRef](#)]
3. Extance, A. Military technology: Laser weapons get real. *Nature* **2015**, *521*, 408–410. [[CrossRef](#)]
4. Bian, Q.; Bo, Y.; Zuo, J.W.; Guo, C.; Xu, C.; Tu, W.; Shen, Y.; Zong, N.; Yuan, L.; Gao, H.W.; et al. High-power QCW microsecond-pulse solid-state sodium beacon laser with spiking suppression and D_{2b} re-pumping. *Opt. Lett.* **2016**, *41*, 1732–1735. [[CrossRef](#)]
5. Meng, S.; Chen, Z.Z.; Bo, Y.; Yuan, L.; Guo, Y.D.; Li, Y.; Lin, Y.Y.; Zhang, L.; Shao, C.F.; Li, W.J.; et al. Thermally-Compensated High Power Nd:YAG Slab Laser Module With Low Wavefront Distortion. *IEEE Photon. Technol. Lett.* **2020**, *32*, 31–34. [[CrossRef](#)]
6. Razdobreev, I.; Shestakov, A. Self-pulsing of a monolithic Tm-doped YAlO₃ Microlaser. *Phys. Rev. A* **2006**, *73*, 053815. [[CrossRef](#)]
7. Krennrich, D.; Knappe, R.; Henrich, B.; Wallenstein, R.; Lhuillier, J.A. A comprehensive study of Nd:YAG, Nd:YAlO₃, Nd:YVO₄ and Nd:YGeVO₄ lasers operating at wavelengths of 0.9 and 1.3 μm. Part 1: CW-operation. *Appl. Phys. B* **2008**, *92*, 165–174. [[CrossRef](#)]
8. Song, Y.J.; Zong, N.; Wang, Z.M.; Jiang, X.X.; Hao, J.J.; Zhang, S.Z.; Wang, X.J.; Bo, Y.; Peng, Q.J. Structure, thermal and spectroscopic properties of Nd:YAlO₃ perovskite crystal between 77 to 300 K for the design of cryogenic cooled solid state laser. *J. Lumin.* **2021**, *237*, 118172. [[CrossRef](#)]
9. Tzeng, Y.S.; Huang, Y.J.; Tang, C.Y.; Su, K.W.; Chen, W.D.; Zhang, G.; Chen, Y.F. High-power tunable single and multi-wavelength diode-pumped Nd:YAP laser in the ⁴F_{3/2}–⁴I_{11/2} transition. *Opt. Express* **2013**, *21*, 26261–26268. [[CrossRef](#)]
10. Yao, B.Q.; Zheng, L.L.; Zhou, R.L.; Duan, X.M.; Zhang, Y.J.; Ju, Y.L.; Wang, Y.Z.; Zhao, G.J.; Dong, Q. Holmium laser in-band pumped by a thulium laser in the same host of YAlO₃. *Laser Phys.* **2008**, *18*, 1501–1504. [[CrossRef](#)]
11. Wu, R.F.; Lai, K.S.; Wong, H.; Xie, W.; Lim, Y.; Lau, E. Multiwatt mid-IR output from a Nd: YALO laser pumped intracavity KTA OPO. *Opt. Express* **2001**, *8*, 694–698. [[CrossRef](#)]
12. Wei, Y.; Zhang, G.; Huang, C.; Zhu, H.; Huang, L.; Ou-yang, X.J.; Wang, G. A single wavelength 1339 nm Nd:YAP pulsed laser. *Opt. Commun.* **2009**, *282*, 4397–4400. [[CrossRef](#)]
13. Yanagida, T.; Akatsuka, M.; Okada, G.; Kawaguchi, N. Optical and scintillation properties of Nd-doped YAlO₃ crystals. *Opt. Mater.* **2019**, *90*, 14–19. [[CrossRef](#)]

14. Song, Y.J.; Xu, Y.Z.; Meng, S.; Jiang, X.; Shao, C.F.; Song, Z.Z.; Zong, N.; Wang, Z.M.; Bo, Y.; Wang, X.J.; et al. Excellent performance of a cryogenic Nd:YAlO₃ laser with low wavefront distortion based on zero thermal expansion. *Opt. Lett.* **2021**, *46*, 2425–2428. [[CrossRef](#)]
15. Huang, Z.; Feng, J.; Pan, W. First-principles calculations of mechanical and thermodynamic properties of YAlO₃. *Comp. Mater. Sci.* **2011**, *50*, 3056–3062. [[CrossRef](#)]
16. Basavalingu, B.; Kumar, M.S.V.; Girish, H.N.; Yoda, S. Hydrothermal synthesis and characterization of rare earth doped yttrium aluminium perovskite R:YAlO₃ (R = Nd, Eu & Er). *J. Alloys Compd.* **2013**, *552*, 382–386.
17. Brik, M.G. Modeling of Optical Properties of 3d and 4f Ions. *J. Electrochem. Soc.* **2009**, *25*, 25–37.
18. Segall, M.D.; Lindan, P.J.D.; Probert, M.J.; Pickard, C.J.; Hasnip, P.J.; Clark, S.J.; Payne, M.C. First-principles simulation: Ideas, illustrations and the CASTEP code. *J. Phys. Condens. Matter* **2002**, *14*, 2717–2744. [[CrossRef](#)]
19. Perdew, J.P.; Burke, K.; Ernzerhof, M. Generalized Gradient Approximation Made Simple. *Phys. Rev. Lett.* **1996**, *77*, 1396. [[CrossRef](#)]
20. Shannon, R.D. Revised effective ionic radii and systematic studies of interatomic distances in halides and chalcogenides. *Acta Crystallogr.* **1976**, *32*, 751–767. [[CrossRef](#)]
21. Diehl, R.; Brandt, G. Crystal structure refinement of YAlO₃, a promising laser material. *Mater. Res. Bull.* **1975**, *10*, 85–90. [[CrossRef](#)]
22. Muñoz-García, A.B.; Anglada, E.; Seijo, L. First-principles study of the structure and the electronic structure of yttrium aluminum garnet Y₃Al₅O₁₂. *Int. J. Quantum. Chem.* **2009**, *109*, 1991–1998. [[CrossRef](#)]
23. Ju, M.; Xiao, Y.; Sun, W.G.; Lu, C.; Yeung, Y.Y. In-Depth Determination of the Microstructure and Energy Transition Mechanism for Nd³⁺-Doped Yttrium Oxide Laser Crystals. *J. Phys. Chem. C* **2020**, *124*, 2113–2119. [[CrossRef](#)]
24. Ju, M.; Huang, J. First-principle study of the microstructure and electronic properties for Cr³⁺ doped yttrium orthoaluminate. *Comput. Mater. Sci.* **2020**, *174*, 109467.
25. Chen, J.; Zhao, G.; Cao, D.; Li, H.; Zhou, S. First-principles calculations of electronic structures and absorption spectra of YAlO₃ crystals with F center. *Comput. Mater. Sci.* **2009**, *46*, 225–228. [[CrossRef](#)]
26. Bercha, D.M.; Rushchanskii, K.Z.; Sznajder, M.; Matkovskii, A.; Potera, P. Elementary energy bands in ab initio calculations of the YAlO₃ and SbSI crystal band structure. *Phys. Rev. B* **2002**, *66*, 195203. [[CrossRef](#)]
27. Herbst, J.F.; Watson, R.E.; Wilkins, J.W. Relativistic calculations of 4f excitation energies in the rare-earth metals: Further results. *Phys. Rev. B* **1978**, *17*, 1689–1701. [[CrossRef](#)]
28. Wu, Z.J.; Zhao, E.J.; Xiang, H.P.; Hao, X.F.; Liu, X.J.; Meng, J. Crystal structures and elastic properties of superhard IrN₂ and IrN₃ from first principles. *Phys. Rev. B* **2007**, *76*, 054115. [[CrossRef](#)]
29. Zhang, L.Z.; Li, Y.K.; Zhou, R.F.; Wang, X.; Wang, Q.S.; Xie, L.Z.; Li, Z.Q.; Xu, B. First-Principles Study of the Effect of Sn Content on the Structural, Elastic, and Electronic Properties of Cu-Sn Alloys. *Crystals* **2023**, *13*, 1532. [[CrossRef](#)]
30. Wu, X.; Qin, S.; Wu, Z.Y. Generalized gradient approximation calculations of the pressure-induced phase transition of YAlO₃ perovskite. *J. Phys. Condens. Matter* **2006**, *18*, 3907–3916. [[CrossRef](#)] [[PubMed](#)]
31. Ross, N.L.; Zhao, J.; Angel, R.J. High-pressure single-crystal X-ray diffraction study of YAlO₃ perovskite. *J. Solid State Chem.* **2004**, *177*, 1276–1284. [[CrossRef](#)]
32. Gaillac, R.; Pullumbi, P.; Coudert, F. ELATE: An open-source online application for analysis and visualization of elastic tensors. *J. Phys. Condens.* **2016**, *28*, 275201. [[CrossRef](#)] [[PubMed](#)]
33. Ravindran, P.; Fast, L.; Korzhavyi, P.A.; Johansson, B.; Wills, J.; Eriksson, O. Density functional theory for calculation of elastic properties of orthorhombic crystals: Application to TiSi₂. *J. Appl. Phys.* **1998**, *84*, 4891–4904. [[CrossRef](#)]

Disclaimer/Publisher’s Note: The statements, opinions and data contained in all publications are solely those of the individual author(s) and contributor(s) and not of MDPI and/or the editor(s). MDPI and/or the editor(s) disclaim responsibility for any injury to people or property resulting from any ideas, methods, instructions or products referred to in the content.